Response to Reviewer #1's Comments

Aeolus is the satellite means for measurements of wind information for the first time, which is the milestone for wind observations for a global scale. In this paper, the authors evaluated the accuracy of wind products of Aeolus with ground-based wind observations from the RWP network in China. The results show that Rayleigh-clear wind products of categories 1 and 2 are better than category 3 with RWP winds, Mie-cloudy wind products are consistent with RWP winds in most of east China. This manuscript is of significance to understand the accuracy of the Aeolus product in China. Overall, this manuscript is clear and well written. However, the following major issues need to be improved:

Response: We thank the anonymous reviewer for his/her comprehensive evaluation and thoughtful comments, which greatly improve the quality of our manuscript. We have made efforts to adequately address the reviewers' concern one by one. For clarity purpose, here we have listed the reviewer' comments in plain font, followed by our response in bold italics.

1. In the introduction part, the author proposes that the significance of this study is to systematically evaluate the accuracy of Aeolus products in the high aerosol background in China for the first time. However, the time of Aeolus products analyzed in this study is from May to September 2020. In this period, the concentration of aerosol in China is generally low. In addition, due to the influence of covid-19 this year, there is little air pollution from May to September, which does not match the hypothesis of "research significance: product accuracy evaluation under the background of high pollution in China". Therefore, is it more reasonable to choose a time with heavy pollution background to reevaluate Aeolus products? What is the author's consideration?

Response: Good questions! It is well recognized that the air quality in China has been significantly improved, largely thanks to the reduction of emission. Meanwhile, the aerosol concentration tends to be low in the summer due to the wet scavenging effect of summer monsoon rainfall. Nevertheless, the summertime PM2.5 in China varies between 30 and 60 μg/m3, depending on the region of

interest (c.f. Fig. 3 in Zhai et al., 2019). This is approximately 3-5 times larger the global mean PM2.5, according to the global comparison analysis (van Donkelaar et al. 2016). Therefore, we think the evaluation of Aeolus wind products in China becomes more scientifically significant, given the high aerosol pollution background in China. In this sense, our study is unique and quite different from most of the validation study in the literature that is mainly limited to region or countries with relatively good air quality. On the other hand, limited availability of Aeolus satellite data prohibits us extending our study to longer time priod, since the Aeolus data went public on May 12, 2020.

As you indicated, the air quality became much better during our study period due to the emission-reduction measures taken by Chinese government in order to combat COVID-19. However, the concentration of pollutants in China is still at a high level during the COVID-19 period, due either to unfavorable meteorological factor, or to the secondary aerosol pollution. For instance, Le et al. (2020) pointed out that up to 90% reduction of certain emissions during the city-lockdown period can be identified from satellite and ground-based observations. Unexpectedly, extreme particulate matter levels simultaneously occurred in northern China. Huang et al., (2020) found that the haze during the COVID lockdown were driven by enhancements of secondary pollution. He et al. (2020) quantitatively studied the impact of the COVID-19 lockdown on China's air pollution. They found that AQI in the locked-down cities was brought down by 19.84 points (PM2.5 down by 14.07 $\mu g\ m^{-3}$) relative to the control group. Despite these improvements, PM2.5 concentrations during the lockdown periods remained four times higher than the World Health Organization recommendations. All of the above-mentioned studies confirmed that China remains plagued with frequent air pollution episodes.

Last but not least, aerosol pollution tends to become most severe in winter in China. The studies regarding how aerosol affects the accuracy of Aeolus wind products in winter merits further investigation in the future.

To clarify this point, we have added some descriptions in the introduction: "For instance, many studies have shown that China experienced several episodes of severe haze pollution during the COVID-19 lockdown period, despite the widespread emission reduction (Huang et al., 2020; He et al., 2020; Le et al., 2020; Su et al., 2020)."

References:

Le, T., Wang, Y., Liu, L., Yang, J., Yung, Y. L., Li, G., & Seinfeld, J. H.: Unexpected air pollution with marked emission reductions during the COVID-19 outbreak in China. Science, 369(6504), 702-706, 2020.

Huang, X., Ding, A., Gao, J., et al.: Enhanced secondary pollution offset reduction of primary emissions during COVID-19 lockdown in China. National Science Review, nwaa137, https://doi.org/10.1093/nsr/nwaa137, 2020.

He, G., Pan, Y., & Tanaka, T.: The short-term impacts of COVID-19 lockdown on urban air pollution in China. Nature Sustainability, 1-7, 2020.

Su, T., Li, Z., Zheng, Y., Luan, Q., and Guo, J.: Abnormally shallow boundary layer associated with severe air pollution during the COVID-19 lockdown in China. Geophys. Res. Lett., 47, e2020GL090041, 2020.

van Donkelaar, A. et al.: Global Estimates of Fine Particulate Matter using a Combined Geophysical-Statistical Method with Information from Satellites, Models, and Monitors. Environ. Sci. Technol. 50, 3762−3772, 2016.

Zhai, S., Jacob, D. J., Wang, X, et al.: Fine particulate matter (PM2.5) trends in China, 2013–2018: separating contributions from anthropogenic emissions and meteorology, Atmos. Chem. Phys., 19, 11031–11041, https://doi.org/10.5194/acp-19-11031-2019, 2019.

2. The paper mentioned the quality of satellite product and ground-based observations, is there any high levels of quality flag in the satellite products? Like low, middle and high? For the ground-based observations, how many 100% confident level data used?

Or how many data were dropped?

Response: To the best of our knowledge, currently there is no high levels of quality flag in the satellite products. At this stage, the Aeolus team only provide the validity flags (0=invalid and 1=valid) and estimated errors (theoretical) as the quality flag.

For the ground-based observations, the confident level is equivalent to valid flag (100%=valid, less than 100%=invalid). As long as it was matched with Aeolus and the confidence is 100%, it has been be used. According to our previous study regarding the introduction of the RWP network in China (Liu et al., 2020), the 100% confident level data accounts for more than 98% of RWP network observation data. Therefore, only about 2% of data were dropped, which has been clarified in section 2 of this revision.

Reference:

Liu, B., Guo, J., Gong, W., Shi, L., Zhang, Y., & Ma, Y.: Characteristics and performance of wind profiles as observed by the radar wind profiler network of China. Atmospheric Measurement Techniques, 13(8), 4589-4600, 2020.

3. What's the meanings of Rayleigh-clear and Mie-cloudy? How do these two algorithms calculate wind information?

Response: The wind observations are classified into Rayleigh-clear wind that refers to the wind in aerosol-poor atmosphere, and Mie-cloudy wind that refers to the wind acquired from Mie backscatter signals induced by aerosols and clouds.

Regarding the algorithms used to estimate wind, the wind speed is calculated based on the Doppler effect. When the laser encounters atmospheric particles (aerosols or molecular), it would produce a Doppler frequency shift. The wind speed can be calculated by detecting this frequency shift. ALADIN is equipped with two different frequency discriminators, namely a Fizeau interferometer that is used to analyze the frequency shift of the narrowband particulate backscatter signal (Mie) and two sequentially coupled Fabry–Pérot interferometers that are used to analyze the frequency shift of the broadband molecular return signal (Rayleigh). Figure R1 illustrates the Doppler effect.

We have added the following paragraph in Section 2.1, which shows as follows: "The wind speed is calculated based on the Doppler effect (Tan et al., 2008). Here, we mainly discuss the performance of Rayleigh-clear winds and Mie-cloudy winds. Rayleigh-clear winds refer to the wind observations in aerosol-free atmosphere, whereas Mie-cloudy winds refer to the winds acquired from Mie backscatter signals induced by aerosols and clouds (Witschas et al., 2020)."

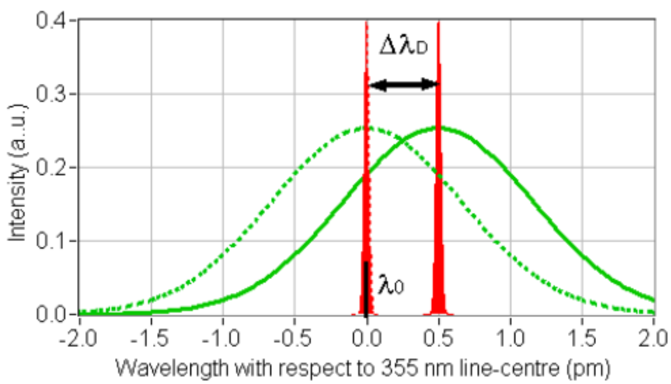

Figure R1. Wavelength spectra for the backscattered Mie (red) and Rayleigh (green) signal for a 355 nm source at λ_0 (dotted lines) and a Doppler shift $\Delta\lambda_D$ (bold lines); the indicated Doppler shift of 0.5 pm corresponds to a LOS wind speed of ~ 200 ms^{-1}

4. What's the estimated errors (x-axis) in the Figure 4? How about all accuracy when using all quality's data (not control the quality using estimated errors)?

Response: The estimated error is theoretical value, which is estimated based on the measured signal levels as well as the temperature and pressure sensitivity of the Rayleigh channel response. It was provided as a separate parameter in the L2B data product. We have added the following descriptions in section 2.1. "The estimated error is a theoretical value, which is estimated based on the measured signal levels as well as the temperature and pressure sensitivity of the Rayleigh channel response (Dabas et al., 2008). It was provided as an indispensable parameter in the L2B data product."

Per your suggestion, we carried out comparison analysis using all quality's data (not control the quality using estimated errors), and the results are shown in Figure R2. It can be found that the correlation is very poor. Therefore, the official documentation and references pointed out that the estimated errors need to be considered when performing data quality control. In addition, we added Figure R2 to the supplementary material. We have added the following sentence in section 2.3: "Figure S1 shows the scatter plots of Aeolus wind speed against RWP wind speed for all data without controlling the quality using estimated errors. It can be found that the correlation is very poor. Therefore, the official documentation and references pointed out that the estimated errors need to be considered when performing data quality control."

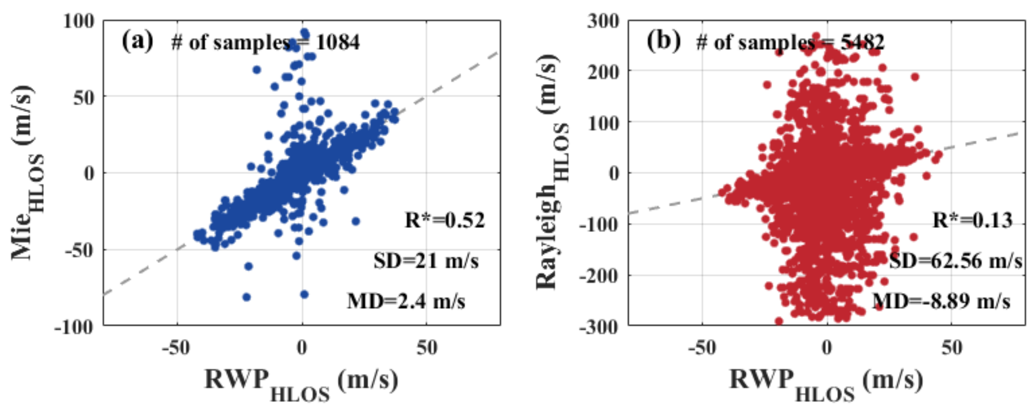

Figure R2. Aeolus against RWP HLOS winds for (a) Mie-cloudy winds and (d) Rayleigh-clear winds for all data.

5. Fig.6 shows a spatial distributions of correlation coefficients for each site. Why coastal areas have larger R values while inner of China has lower R values? Especially in the Sichuan basin.

Response: Good question! The RWP instruments have been updated in coastal provinces in China in recent years, and most of the RWP sites are concentrated along the coastal areas, where have relatively rapid economic development speed. Coincidently, the sites with high R values mostly lie at these regions. Therefore, the maintenance capability at these sites is likely to the major reason for the spatial variability of R values found in Fig. 6.

Another reason may be the small number of sample points of these inland sites (Figure R3), which affects the correlation results.

To clarify this issue, we have added the following sentence in section 3.1: "Therefore, the reason for the high R values observed here could be the sufficient maintenance of RWP instrument along the coastal region, resulting to more matched data points therein (Figure S2)."

6. Number of points of each site for validation of winds are important in calculating R, and SD, etc., some sites show a lower R values (e.g. Sichuan basin) in the Figure 6. So, what's the number of each site used in the validation? Give a spatial distribution of each site's number of paired data.

Response: Points taken! We added the Figure R3 to the supplementary material.

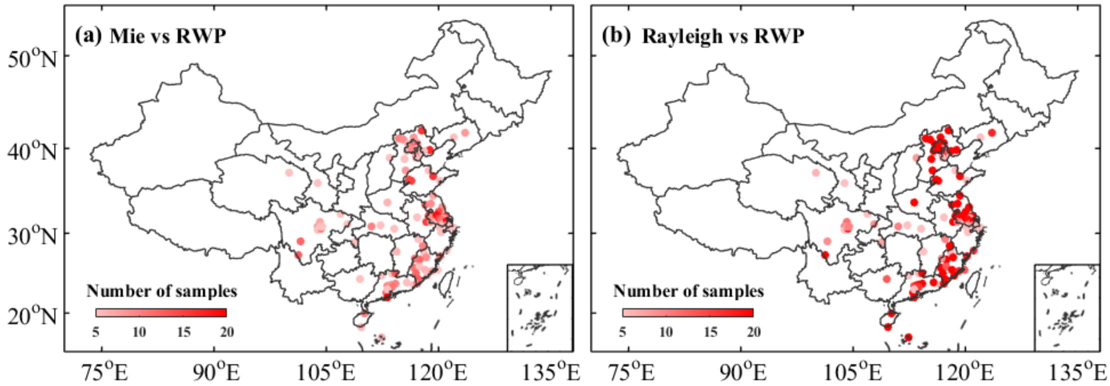

Figure R3. Spatial distribution of each site's number of paired data between Aeolus HLOS and RWP HLOS wind speeds. The wind measurements are separated in (a) Mie-cloudy winds and (b) Rayleigh-clear winds.

7. Why Rayleigh wind in the descending has a large error than ascending in the 0–2 km in the Figure 11 (b, c)?

Response: This may be caused by the diurnal variation of aerosols in the atmospheric boundary layer. At ascending time (06:00 LST), the boundary layer height is generally less than 0.5 km (Guo et al., 2016), and the atmosphere in the range of 0.5–2 km is dominated with molecule scattering. By comparison, at descending time (18:00 LST), the boundary layer height tends to be elevated to approximately 1–2 km, in which aerosol scattering dominates. It is noteworthy that the Rayleigh performance is largely limited by received power. Nevertheless, the strong aerosol scattering in the boundary layer would inevitably undermine the molecular scattering signal, thereby reducing the inversion accuracy of Rayleigh wind from Aeolus (Tian et al., 2017).

Related discussion has been added to this revision.

Response to Reviewer #2’s Comments

This Technical Note systematically compared the Mie-cloudy and Rayleigh-clear wind products from Aeolus measurements with wind observations from the radar wind profiler (RWP) network in China. The topic is very interesting and has important implications in evaluating the quality of Aeolus observation and applications over China regions. The paper is well organized and written. The findings of this study are worth of publication in the journal after minor revision as following:

Response: We greatly appreciated the reviewer’s positive comments on our manuscript, which greatly improve the quality of our manuscript. We have made efforts to adequately address the reviewers' concern one by one. For clarity purpose, here we have listed the reviewer' comments in plain font, followed by our response in bold italics.

1. P4:” Over countries or regions with episodes of extensive heavy air pollution, such as China, the high aerosol concentrations could significantly affect satellite observations, which in turn can affect the accuracy of wind products and their applications in weather forecast and climate prediction.” Some references should be added to support this deduction. How high aerosol concentrations could significantly affect satellite observations?

Response: The potential impact induced by high aerosols concentrations is at least twofold: On one hand, in the presence of dense smoke, dense fog, and haze, the laser energy of ALADIN/Aeolus, which is a spaceborne Doppler lidar, would be attenuated, making it unable to obtain near-surface observation signals (Winker et al., 2009). On the other hand, when the aerosol scattering signal is too strong, and thus the molecular scattering signal will be masked, which in turn impair the signals used to retrieve Rayleigh wind (e.g., Tian et al., 2008; 2017).

Per your suggestion, the above-mentioned descriptions have been incorporated into Section 1 in this revision as follows:

"In particular, in the atmosphere fraught with dense smoke, dense fog, and haze, the laser energy would be attenuated, making it likely not to well obtain near-surface observation signals (Winker et al., 2009). Moreover, when the aerosol scattering signal is too strong, the molecular scattering signal will be dramatically attenuated, thereby undermining the inversion of Rayleigh wind (Tian et al., 2008; 2017). For instance, many previous studies have shown that China experienced several episodes of severe haze pollution during the COVID-19 lockdown period, despite the widespread emission reduction (Huang et al., 2020; He et al., 2020; Le et al., 2020; Su et al., 2020)."

References:

Winker, D. M., Vaughan, M. A., Omar, A., Hu, Y., Powell, K. A., Liu, Z., Hunt, W. H., and Young, S. A.: Overview of the CALIPSO mission and CALIOP data processing algorithms, J. Atmos. Ocean. Tech., 26, 2310–2323, 2009

Tan, D. G. H., Andersson, E., de Kloe, J., Marseille, G., Stoffelen, A., Poli, P., Denneulin, M., Dabas, A., Huber, D., Reitebuch, O., Flamant, P., Le Rille, O., and Nett, H.: The ADM-Aeolus wind retrieval algorithms. Tellus A, 60, 191–205, 2008.

Tan, D., Rennie, M., Andersson, E., Poli, P., Dabas, A., de Kloe, J., Marseille, G.-J., and Stoffelen, A.: Aeolus Level-2B Algorithm Theoretical Basis Document, Tech. rep., AE-TN-ECMWFL2BP-0023, v. 3.0, 109 pp., 2017.

2. P6: "To achieve a synchronization, the time difference between the RWP and Aeolus wind profiles should be minimum". How do you define the minimum? Please clarify it.

Response: Good comment! The time difference between Aeolus and RWP profile is required to be within 10 minutes. We modified this sentence to: "To achieve a synchronization, the time difference between the RWP and Aeolus wind profiles is required to be less than 10 min.".

3. P7: What is the reason that you distinguished and employed ascending orbit and descending orbit data to discuss their accuracy? R fallen? May influence the comparison results?

Response: Good question! To the best of our knowledge, at least the following two concerns justify the distinguishing between ascending orbit and descending orbit data when comparison is performed.

First of all, IR and UV radiation, along with the aerosol and cloud, show significant diurnal variability, which is supposed to exert influence on the signals of Aeolus.

Second, the descending and ascending orbit data, corresponding to the sunrise and sunset times, are provided to the public separately, and thus the readers are eager to know their corresponding accuracy.

Actually, our results showed that there existed difference of the accuracy of Aeolus wind product between descending and ascending orbit data, justifying the validation methods used in our study.

4. P8-9: the variables in equations 4-6 should be clarified.

Response: Amended as suggested.

5. P24: Table 1 caption: 75km-radius–>75-km radius

Response: Amended as suggested.

6. Figure 1: The flag of geographic direction should added

Response: Per your suggestion, north **arrow** ***has been added in Fig.1.***

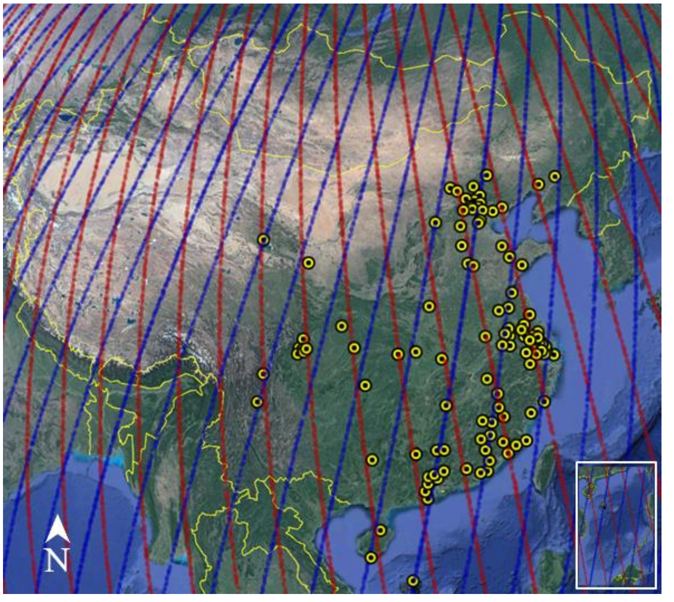

7. Figure 3: The flag of geographic direction is unclear.

Response: The flag of geographic direction has been enlarged as suggested. See the following figure, please.

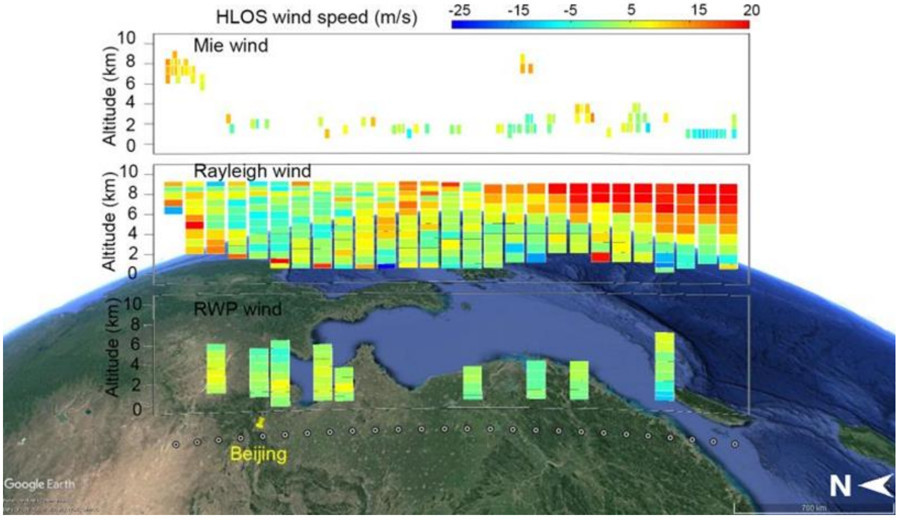

Technical Note: First comparison of wind observations from ESA's satellite mission Aeolus and ground-based Radar wind profiler network of China

Jianping Guo[1], Boming Liu[2*], Wei Gong[2], Lijuan Shi[3], Yong Zhang[3], Yingying Ma[2], Jian Zhang[4], Tianmeng Chen[1], Kaixu Bai[5], Ad Stoffelen[6], Gerrit de Leeuw[6], and Xiaofeng Xu[7]

[1] The State Key Laboratory of Severe Weather, Chinese Academy of Meteorological Sciences, Beijing 100081, China
[2] State Key Laboratory of Information Engineering in Surveying, Mapping and Remote Sensing (LIESMARS), Wuhan University, Wuhan, China
[3] Meteorological observation Centre, Chinese Meteorological Administration, Beijing 100081, China
[4] Hubei Subsurface Multi-Scale Imaging Key Laboratory, Institute of Geophysics and Geomatics, China University of Geosciences, Wuhan 430074, China
[5] School of Geographic Sciences, East China Normal University, Shanghai 200241, China
[6] The Royal Netherlands Meteorological Institute (KNMI), 3730 AE De Bilt, The Netherlands
[7] Chinese Meteorological Administration, Beijing 100081, China

Correspondence to: Boming Liu (liuboming@whu.edu.cn)

Abstract. Aeolus is the first satellite mission to directly observe wind profile information on a global scale. After implementing a set of bias corrections, the Aeolus data products ~~has gone~~went public on 12 May 2020. However, Aeolus wind products over China were thus far not evaluated extensively by ground-based ~~in-situ~~remote sensing measurements ~~comparison~~. In this study, the Mie-cloudy and Rayleigh-clear wind products from Aeolus measurements are validated against wind observations from the radar wind profiler (RWP) network in China. Based on the position of each RWP site relative to the closest Aeolus ground tracks, three matchup categories are proposed and comparisons between Aeolus wind products and RWP wind observations are performed for each category separately. The performance of Mie-cloudy wind products does not change much between the three matchup categories. On the other hand, for Rayleigh-clear and RWP wind products, c~~C~~ategories 1 and 2 are found to have much smaller differences, compared with category 3. This could be due to the RWP site being sufficiently approximate to Aeolus ground track for categories 1 and 2. In the vertical, the Aeolus wind products are similar to the RWP wind observations, except for the Rayleigh-clear winds

in the height range of 0−1 km. The mean absolute normalized differences between the Mie-cloudy (Rayleigh-clear) and the RWP wind components are 3.06 (5.45), 2.79 (4.81), and 3.32 (5.72) m/s at all orbit times, ascending, and descending Aeolus orbit times, respectively. This indicates that ~~the observation time has a minor effect on the comparison, and~~ the wind products for ascending orbits are ~~is~~ slightly superior to those~~at~~ for descending orbits, and the observation time has a minor effect on the comparison. From the perspective of spatial differences, the Aeolus Mie-cloudy winds are consistent with RWP winds in most of east China, except in coastal areas where the Aeolus Rayleigh-clear winds are more reliable. Overall, the correlation coefficient R between Mie-cloudy (Rayleigh-clear) wind ~~products~~ and RWP wind component observation~~s~~ is 0.94 (0.81),~~.~~ suggesting ~~This indicates~~ that Aeolus wind products are in good agreement with wind observations from the ~~radar wind profiler~~RWP network in China. The findings give us sufficient confidence in assimilating the newly released Aeolus wind products in operational weather forecasting in China.

1 Introduction

Observations of atmospheric wind profiles are essential to the prediction of extreme rainfall events (Nash and Oakley, 2001; Huuskonen et al., 2014; King et al., 2017), the forecasting of tropical cyclones and hurricanes (Pu et al., 2010; Stettner et al., 2019), a better understanding of persistent haze pollution episodes (Liu et al., 2018; Yang et al., 2019; Zhang et al., 2014; 2020; Huang et al., 2020) and complicated aerosol-cloud-precipitation interactions (Li et al., 2011; Lebo and Morrison, 2014; Guo et al., 2018; 2019; Huang et al., 2019). Moreover, under the influence of large-scale dynamic forcing and land surface processes, wind speed and direction will vary dramatically, both temporally and spatially, which poses a large challenge for models to simulate or forecast the variation of wind very well (Weissmann, et al., 2007; Michelson and Bao, 2008; Constantinescu et al., 2009). Particularly, the winds in the atmospheric boundary layer are mostly turbulent and hard to be well reproduced by models without assimilation of wind observations (Belmonte and Stoffelen, 2019; Benjamin et al., 2004; Simonin et al., 2014; Liu et al., 2017; Stoffelen et al., 2017). Therefore, continuous global wind profile observations are of great significance for advancing our knowledge of atmospheric dynamics as well as for improving the accuracy of numerical weather prediction (Stoffelen et al., 2006).

To this end, various instruments have been developed to measure wind speed and direction, including radiosondes, radar wind profilers (RWP), and geostationary satellites (Stoffelen et al., 2019; Bentamy et al., 1999; Draper and Long 2002; Guo et al., 2016; Liu et al., 2019). Among others, radiosonde measurements are one of the most widely used observations for atmospheric wind profiles (Houchi et al., 2010). Radiosondes can directly measure vertical profiles of thermodynamic and dynamic parameters, including pressure, temperature, humidity, and horizontal winds. Nevertheless, the launch frequency of operational radiosonde balloons is not high, only once or twice a day (Guo et al., 2016) and spatially sparse. Therefore, the advantage of the use of RWPs for characterizing the temporal variability of the wind is its continuous and unattended operation (~~Zhang et al., 2020;~~ Liu et al., 2020a~~19~~; Zhang et al., 2020). However, the operational and maintenance costs are extremely high, and the spatial coverage (both vertically and horizontally) is still limited, such that operation of most of the nation-wide radar wind profiler (RWP) networks has stopped, except in China (Guo et al., 2016; Liu et al., 2020b~~a~~). In comparison, a spaceborne Doppler wind lidar (DWL) is increasingly considered as one of the most promising instruments to meet the need of near-real time observations, mostly thanks to its global coverage (Stoffelen et al., 2020; Zhai et al., 2020).

Aeolus, launched on 22 August 2018, is the first ever satellite designed to directly observe line-of-sight wind profiles on a global scale (Stoffelen et al., 2006; Witschas et al., 2020; Zhai et al., 2020). The unique payload, the Atmospheric LAser Doppler INstrument (ALADIN), is a direct detection ultraviolet wind lidar operating at 355 nm (Reitebuch, 2012; ESA, 2016). It uses a dual channel design, which can simultaneously obtain the particulate and molecular backscatter from Mie and Rayleigh channels, respectively. Aeolus provides one component of the wind vector along the instrument line-of-sight (Stoffelen, 2006). The Aeolus dataset has gone through bias correction procedures and is available publicly to forecasting services and scientific users since 12 May 2020. Currently, the products that are entirely publicly accessible are the Level 1B and 2B products. Here, the Level 2B products~~,~~ containing the horizontal line of sight (HLOS) wind observations are~~is~~ used. The Level 2B product provides the scientific wind product for users, which is the geo-located and consolidated HLOS wind observation with actual atmospheric correction and bias corrections applied (Tan et al., 2017; Rennie et al., 2018).

To estimate the performance of the Aeolus wind products, the Aeolus team has performed extensive experimental (e.g., Witchas et al., 2010) and simulation studies (Marseille et al., 2003; Stoffelen et al., 2006), which were complemented by a series of airborne DWL measurements (Lux et al., 2018; Marksteiner et al., 2018; Witschas et al., 2020). The first validation of the Aeolus Level 2B product was done against the European Centre for Medium-Range Weather Forecasts (ECMWF) Numerical Weather Prediction (NWP) model, which played a crucial role in the Aeolus characterization (Rennie and Isaksen, 2020). Validation against in-situ airborne DWL measurements were conducted by Witschas et al. (2020). They analyzed the systematic and random errors of the Aeolus wind products and confirmed the necessity to validate the Aeolus wind product. Lux et al. (2020) compared the wind observations from Aeolus and the ALADIN Airborne Demonstrator (A2D) with the ECMWF NWP winds and found that the biases of the A2D and Aeolus line-of-sight wind speeds were −0.9 m/s and +1.6 m/s, respectively, while the random errors were around 2.5 m/s. In a triple collocation, Albertema (2019) used a spatially dense airplane network for in-situ verification of Aeolus wind profiles. The above-mentioned verification exercises have deepened our understanding of the global Aeolus wind products and most of the biases have now been corrected in the newest L2B Aeolus product release (see next section). It is noted that most in-situ verifications were conducted over Europe. Over countries or regions with episodes of extensive heavy air pollution, such as China, the high aerosol concentrations could ~~significantly~~ affect satellite observations, which in turn can potentially affect the accuracy of wind products and their applications in weather forecast and climate prediction. In particular, in the atmosphere fraught with dense smoke, dense fog, and haze, the laser energy would be attenuated, making it likely not to well obtain near-surface observation signals (Winker et al., 2009). Moreover, when the aerosol scattering signal is too strong, the molecular scattering signal will be dramatically attenuated, thereby undermining the inversion of Rayleigh wind (Tian et al., 2008; 2017). For instance, many previous studies have shown that China experienced several episodes of severe haze pollution during the COVID-19 lockdown period, despite the widespread emission reduction (Huang et al., 2020; He et al., 2020; Le et al., 2020; Su et al., 2020). For this reason, among others, it is worthwhile to extend the in-situ verification of the performance of Aeolus wind products to China.

In this study, the quality of the Aeolus wind products over China is investigated by comparing them with the wind observations from the RWP network in China. For the comparison of the RWP measurements with the Aeolus results, the RWP sites are divided into three categories according to the geographic coordinates of each RWP site relative to the nearest Aeolus ground tracks categories. The HLOS wind profile differences between Aeolus and RWP winds are analysed for each site. The paper is organized as follows. First, the Aeolus and RWP data used in this study are briefly described, and the data matching algorithms are addressed in detail in Section 2. The subsequent sections present a comprehensive comparison between the Aeolus wind products and the RWP wind observations. In Section 4, the main findings are summarized.

2 Data and methods

2.1 Aeolus wind observations

Aeolus is the first mission to acquire atmospheric wind profiles on a global scale, deploying the satellite-borne DWL system ALADIN (Stoffelen et al., 2005; ESA, 2008; Reitebuch, 2012). Aeolus flies in a sun-synchronous orbit at an altitude of about 320 km, with a 7-day repeat cycle. The ground tracks of Aeolus over China are shown in Figure. 1. The red and blue lines represent the ascending and descending ground tracks at 06:00 and 18:00 Local Solar Time (LST), respectively. The Aeolus L2B wind product data are the mission's prime and increasingly receive attention. Typically, the Aeolus wind profiles from the ground up to 30 km altitude refer to the wind vector component along the instrument's line-of-sight, with a vertical resolution of 0.25 to 2 km and a wind accuracy of 2 to 4 m/s, depending on the altitude (Rennie et al., 2020). In this study, the Aeolus Level 2B (L2B) products from 20 April 2020 to 20 July 2020 are collected for comparison with RWP observations. They contain the HLOS winds for the Mie and Rayleigh channels. The auxiliary data, such as validity flag, estimated error, top and bottom altitudes of vertical bin, etc., are also given in the Aeolus L2B product. The wind speed is calculated based on the Doppler effect (Tan et al., 2008). Here, we mainly discuss the performance of Rayleigh-clear winds and Mie-cloudy winds. Rayleigh-clear winds refer to the wind observations in aerosol-free atmosphere. Mie-cloudy winds refer to the winds acquired from- Mie backscatter signals induced by aerosols and clouds ~~particulate backscatter, predominatly from clouds~~ (Witschas et al., 2020). The quality of the Aeolus wind data is indicated by validity flags (0=invalid and 1=valid) and estimated errors (theoretical). The estimated error is a theoretical value, which is estimated based on the measured signal levels as well as the temperature and pressure sensitivity of the Rayleigh channel response (Dabas et al., 2008). It was provided as an indispensable parameter in the L2B data product. More detailed descriptions are provided in previous studies (De Kloe et al., 2017; Tan et al., 2017).

2.2 RWP wind observations

The RWP network in China is operated and maintained by the China Meteorological Administration. It comprises 134 stations until April 2020 and is designed primarily for measuring winds at various altitudes (Liu et al., 2020b). The RWP can almost continuously operate (24/7), acquiring vertical profiles of horizontal wind speed, wind direction and vertical velocity over the station (Zhang et al., 2019; Liu et al., 2019). The temporal and spatial vertical resolutions of RWP data are 6 min and 120 m, respectively. The maximum detection height ranges from 3 to 10 km. The quality flag of the data is based on confidence level, that is, a 100% confidence level indicates that the data are valid (Liu et al., 2020b). It should be noted that only about 2% of RWP measurements were dropped for further analysis here, and more detailed information on the RWP network and its data quality can refer to Liu et al. (2020b). Due to the fact that the distance between adjacent tracks of Aeolus is relatively large, subsequent processes are applied to screen the RWP sites. The sites that are more than 1 ° away from the Aeolus ground track are removed. Following this procedure, 109 stations were selected for comparison with Aeolus data (yellow dots in Figure~~.~~ 1). For each of these stations, the horizontal wind speed and direction measured during the period from 20 April 2020 to 20 July 2020 were obtained to compare them with the results from Aeolus.

2.3 Data matching procedures

Regarding the different spatial-temporal resolutions of RWP and Aeolus, data matching procedures are necessary before comparing. A flowchart of the procedures is shown in Figure 2. First, the RWP data and Aeolus data need to be matched in both time and space. To achieve a synchronization, the time difference between the RWP and Aeolus wind profiles is required to be less than 10 min. Meanwhile, referring to the well-established geographical matching principle (Zhang et al., 2016), the distance between an Aeolus wind profile and ~~a~~an RWP site should be less than 75 km. After temporal and spatial collocation, the closest Aeolus observation to each RWP measurement is adopted for a comparison.

In a next step, the valid RWP wind speed and direction are extracted from the wind profile when the data has 100% confidence level (Liu et al., 2020b). Moreover, by matching the lowest and highest extracted RWP data with Aeolus, the overlapping wind profiles are selected. In addition, when the altitude coverage of RWP cannot completely match the detection range of the Aeolus, which is typically from 0 to 30 km, a threshold for the number of available RWP observations within an Aeolus bin has to be set. For each Aeolus vertical bin, all of the heights should be covered by RWP measurements. The RWP wind vector in each bin is then projected onto the Aeolus HLOS using the following equation (Witschas et al., 2020):

$$v_{RWP_{HLOS}} = \cos(\psi_{Aeolus} - wd_{RWP}) \cdot ws_{RWP} \tag{1}$$

where ψ_{Aeolus} represents the Aeolus azimuth angle which is given by the Aeolus L2B data product; ws_{RWP} and wd_{RWP} are the RWP wind speed and direction, respectively. For further comparison, the $v_{RWP_{HLOS}}$ in each bin are averaged to compare with Aeolus HLOS winds.

In addition, the Aeolus winds are acceptable only when the validity flag equals 1 and the estimated errors for wind are, respectively, less than 7 and 5 m/s for Rayleigh and Mie channels. The flag and error information are provided as parameters in the L2B data product, and the error is estimated based on the measured signal levels as well as the temperature and pressure sensitivities of the Rayleigh channel response (Dabas et al., 2008). Figure S1 shows the scatter plots of Aeolus wind speed against RWP wind speed for all data without controlling the quality using estimated errors. It can be found that the correlation is very poor. Therefore, the official documentation and references pointed out that the estimated errors need to be considered when performing data quality control. The selection of the thresholds is described in detail in the next section.

A case study of comparison between ~~for~~ the Aeolus wind measurements and RWP wind observations on 28 April 2020 is presented in Figure 3, which is superimposed on ~~shows~~ a Google Earth map of ~~north~~ East China ~~in which~~where the Aeolus ground track is marked as white circles and the track passes through nine RWP sites. Top and middle panels show the Aeolus Mie-cloudy and Rayleigh-clear winds that pass the valid flag and estimated error selection procedures. The bottom panel displays the corresponding RWP winds matched to the Aeolus Rayleigh-clear measurement grid. It is noted that the horizontal resolution (available observations) of the Mie-cloudy wind products is finer (higher) than that of the Rayleigh wind products. Most of the RWP wind observations are consistent with the Rayleigh wind measurements.

2.4 Statistical method

The HLOS difference between Aeolus HLOS winds ($v_{Aeolus_{HLOS}}$) and the corresponding $v_{RWP_{HLOS}}$ is given by:

$$v_{diff} = v_{Aeolus_{HLOS}} - v_{RWP_{HOLS}} \tag{2}$$

Following Witschas et al. (2020), Aeolus winds with a large estimated error should be removed prior to their use in our analysis. A sensitivity analysis is conducted to choose a suitable threshold for the estimated value of error (Figure 4). For both Mie-cloudy and Rayleigh-clear winds (Figures~~s.~~ 4a~~,~~b), the v_{diff} between RWP and Mie-cloudy winds is within a rather small margin for estimated errors smaller than 7 m/s and increases with increasing error for higher values. In particular, the v_{diff} between RWP and Rayleigh-clear winds is a rather constant when the error is less than 10 m/s and increases remarkably for the error exceeding 10 m/s. Therefore, referring to the previous threshold standard (Witschas et al., 2020), the selected threshold value for the error is 5 m/s for Mie-cloudy wind and 7 m/s for Rayleigh-clear wind.

Due to the number of samples are limited, which may affect the statistical significance of the comparative results. Therefore, to better evaluate the performance of $v_{Aeolus_{HLOS}}$, the Aeolus-RWP HLOS differences are normalized by dividing by the theoretical standard deviation (SD) of Aeolus estimated error. It can be expressed by:

$$v_{N\_diff} = v_{diff} \;/\; SD_{estimated\ error} \tag{3}$$

Moreover, to evaluate the comparative results, the mean difference (MD) and SD of v_{N_diff} are estimated according to:

$$\mathrm{MD} = \frac{1}{n}\sum_{i=1}^{n} v_{N\_diff} \tag{4}$$

and

$$\mathrm{SD} = \sqrt{\frac{1}{n-1}\sum_{i=1}^{n}(v_{N\_diff} - MD)^2} \tag{5}$$

w~~W~~here v_{N_diff} is the normalized difference between Aeolus and RWP HLOS wind speed. The correlation coefficient (R) between RWP and Aeolus winds is calculated by:

$$R = \frac{\sum_{i=1}^{n}(x_i-\bar{x})(y_i-\bar{y})}{\sqrt{\sum_{i=1}^{n}(x_i-\bar{x})^2}\sqrt{\sum_{i=1}^{n}(y_i-\bar{y})^2}} \tag{6}$$

w~~W~~here x_i and y_i represent the i-th sample point of Aeolus and RWP wind speed dataset, respectively. ~~The~~ $\bar{x}$ and $\bar{y}$ represent the mean wind speed of Aeolus and RWP wind speed dataset, respectively.

3 Results and discussion

3.1 Comparison of Aeolus and RWP wind observations

Scatter plots of Aeolus wind speed against RWP wind speed for Mie-cloudy winds and Rayleigh-clear winds at different times are presented in Figure~~.~~ 5. The blue and red dots represent the Mie-cloudy and Rayleigh-clear winds, respectively. The Aeolus data were recorded from April to July 2020 and provide 817 (2430) samples for comparison of Mie-cloudy (Rayleigh-clear) and RWP winds with RWP observations. Figure~~s.~~ 5a-c shows that the slopes of linear fits of Mie-cloudy vs RWP winds are 1.01, 0.9 and 1.04 for all data, ascending and descending orbits, respectively. R between Mie-cloudy and RWP winds are 0.94, 0.9 and 0.9 for all data, ascending and descending orbits, respectively. These results indicate that the Aeolus Mie-cloudy wind products are broadly consistent with RWP wind observations over China. Figure~~s.~~ 5d-f illustrates that for Rayleigh-clear winds, the slopes of linear fit (values of R) are 0.91 (0.74) and 0.96 (0.72) for ascending and descending orbits, respectively. Overall, for all data, the slopes of the linear fits and the R values for the Rayleigh-clear winds are 0.99 and 0.81, respectively. These results indicate that the performance of the Aeolus Rayleigh-clear wind products is reliable over China. It also finds that the performance of Mie-cloudy wind products is superior to that of Rayleigh-clear wind products. In addition, it is interesting to note that most of wind speeds are positive during the ascending and negative at descending, due to the predominant westerly wind component.

The correlation coefficients between the Aeolus and RWP winds for each site are shown in Figure~~.~~ 6, in which black circles denote the sites that pass the significance test (P<0.05). It is noted that for some sites the number of valid samples is smaller than 5 which is too small for a statistically valid comparison. Ultimately, we obtain the spatial distribution of the number of paired data samples, which is shown in Figure S2~~1~~. For Mie-cloudy wind products, a total of 72 sites can provide the comparison result and 53 of them have a correlation coefficient (R) exceeding 0.8, thus indicating that the Aeolus Mie-cloudy wind products are consistent with RWP wind observations in most regions of east China. For the Rayleigh-clear wind products, 89 sites provide comparison results, but for only 27% of them R is larger than 0.8 and for 70% R is larger than 0.6. This indicates that the performance of the Aeolus Rayleigh-clear wind products is lower than that of Mie HLOS winds, as found elsewhere too (Rennie and Isaksen, 2020). The geographical distribution in Figure~~.~~ 6b shows that the sites with high ~~correlation coefficients~~R values are mainly located in coastal areas where economic development is much faster. These results indicate that the HLOS distributions may be wider in the coastal regions, leading to higher correlations. Therefore, the reason for the high R values observed here could be the sufficient maintenance of RWP instrument along the coastal region, resulting to more matched data points therein (Figure S2~~1~~).

3.2 RWP station type

According to the geographic location of each RWP site relative to its nearest Aeolus ground tracks, all the RWP sites are divided into three categories, as shown in Figure 7, in which the red triangle represents the RWP site and the black circle shows an area with a radius of 75 km centred on the RWP site. Category 1 demonstrates the RWP sites matched to two Aeolus ground tracks, with the nearest distance between the RWP site and the Aeolus ground track less than 37.5 km. In addition, category 2 denotes the RWP sites matched by one Aeolus ground track, with the nearest distance less than 37.5 km. Category 3 is the same as category 2 except that the nearest distance is larger than 37.5 km. From all 109 RWP sites, 39 can be attributed to category 2, indicating that 36 % of the RWP sites closely match up with the Aeolus profiles based on their shortest distance of less than 37.5 km. In contrast, categories 1 and 3 have less matchups, i.e. 32 sites (29 %) for category 1 and 38 sites (35 %) for category 3. The details of the classification criteria are tabulated in Table 1, in which the number of Aeolus ground tracks, RWP sites, and the shortest distance between them are summarized.

Figure 8 shows the geographic locations of the RWP sites for categories 1, 2, and 3 (cyan, green, and blue solid circles are for 1, 2, 3 resp.). It is notable that the geographical distributions of categories 1 and 3 are broadly scattered across central and eastern China but category 2 is more predominant over the coastal areas. In addition, we note that the shortest distances in categories 1 and 2 are both less than 37.5 km and therefore, in total 71 sites with a sufficient approximation to the Aeolus ground tracks are available weekly. This condition indicates that the RWP network in China is well suited for comparison with Aeolus observations.

3.3 Differences between Aeolus and RWP winds

The wind speed normalized differences between Mie-cloudy winds and RWP winds are shown in Figure~~.~~ 9. It is noted that some sites cannot provide comparison results due to empty sample points. The text labels represent the mean difference and standard deviation of the normalized differences in each category. For more than half of the sites (52 out of 90, i.e., 58 %), the mean normalized difference is negative, and the mean normalized difference for all sites is -0.38 ± 4.19 m/s, indicating a small underestimation by Aeolus. More specifically, the mean normalized differences for category 1, 2, and 3 are -0.33 ± 4.13, -0.26 ± 3.83, and -0.55 ± 4.66 m/s, respectively, implying that the maximum normalized difference among the categories could be as large as 9 m/s. The ascending/descending HLOS wind normalized differences are presented in Figures~~.~~ 9e-f. We note that the Aeolus LOS points to the right of the spacecraft into the dark side of the earth, implying a westward viewing direction in the morning (descending) and an eastward viewing direction in the evening (ascending). In addition, note that the climatological weather conditions are different in the morning and the evening. More than half of the RWP sites (28 out of 50, i.e., 56%) have positive differences in mean HLOS during ascending, and for most of the sites (37 out of 53, i.e., 70%) they are negative during the descending orbits. The mean normalized differences are 0.1 ± 3.84 and -0.83 ± 4.5 m/s for ascending and descending observations, respectively, which suggest that the observation time has a minor effect on the performance of Mie-cloudy winds.

For Rayleigh-clear winds, the normalized HLOS differences between Aeolus and RWP are presented in Figure~~.~~ 10. Overall, the Rayleigh-clear winds are a bit underestimated as evidenced by the negative differences for most of RWP sites (66 of out 94, i.e., 70%) and their mean value over all sites is -0.77 ± 7.34 m/s (statistically insignificant differences). Moreover, the mean normalized difference for Category 3, has a larger magnitude (1.31 m/s), as compared with categories 1 (0.21 m/s) and 2 (0.85 m/s). These differences indicate that the sample size might have some effect on the HLOS differences for the Rayleigh-clear winds. For the ascending orbit differences at over half of the RWP sites (34 out of 57, i.e., 59%) have negative values, with a mean of -0.04 ± 6.29 m/s. Similarly, for descending orbits, 71% of the RWP sites (42 out of 59 sites) have negative values, with a mean of -1.14 ± 7.22 m/s, i.e., statistically insignificant biases. This result moreover indicates that the performance of Rayleigh-clear winds is slightly affected by the observation time.

Figure 11 shows the vertical distribution of the normalized differences between the Aeolus HLOS wind speed and the RWP HLOS wind speed for different categories and times, in which the shadow area represents the standard deviation at different altitudes and the blue and red lines represent Mie-cloudy and Rayleigh-clear winds, respectively. For all observation times, the maximum mean normalized difference between the Mie-cloudy (Rayleigh-clear) winds and the RWP winds is 1.78

(3.23) m/s in the height range of 7−8 (0.3−1) km. Overall, the mean normalized difference between the Mie-cloudy (Rayleigh-clear) winds and the RWP winds is less than 2 m/s in the height range of 1−9 km. These results show that the biases of the Mie-cloudy and Rayleigh-clear wind products are acceptable in the height range of 1−9 km. Note that the Rayleigh-clear wind products have a large difference (3.23±17 m/s) in the height range of 0−1 km. It is due to the Rayleigh performance is limited by received power. Combined with Figures~~.~~ 11b and 11c, the vertical distributions of the wind speed normalized differences during ascending and descending orbits are opposite to each other, indicating that the changes in observation time could exert influences on the vertical distribution of the wind speed difference. This may be caused by the diurnal variation of aerosols in the atmospheric boundary layer. At ascending time (06:00 LST), the boundary layer height is generally less than 0.5 km (Guo et al., 2016), and the atmosphere in the range of 0.5–2 km is dominated with molecule scattering. By comparison, at descending time (18:00 LST), the boundary layer height tends to be elevated to approximately 1–2 km, in which aerosol scattering dominates. It is noteworthy that the Rayleigh performance is largely limited by received power. Nevertheless, the strong aerosol scattering in the boundary layer would inevitably undermine the molecular scattering signal, thereby reducing the inversion accuracy of Rayleigh wind from Aeolus (Tian et al., 2017). These conclusions can also apply to the vertical distribution of the differences in all categories. For Mie-cloudy wind products, the normalized differences are underestimated in the region 7–9 km for categories 1 and 3, while for Category 2, they are overestimated in the height range of 7−9 km. Rayleigh-clear wind products are overestimated in the altitude interval of 4–6 km for categories 1 and 2 and underestimated over the full vertical range for category 3. Again, the statistical significance is low.

More statistics with regard to the mean absolute normalized difference between Aeolus and RWP winds are presented in Figure~~.~~ 12. From the perspective of observation time, the mean absolute normalized difference between the Mie-cloudy (Rayleigh-clear) and RWP wind speeds are 3.06±2.89 (5.45±4.97), 2.79±2.64 (4.81±4.06), and 3.32±3.15 (5.72±4.55) m/s for all data, ascending orbits, and descending orbits, respectively. These results suggest that the observation time has a minor effect on the HLOS comparison, and the wind products for ascending orbits is slightly superior to that for descending orbits. As for another relevant variable, i.e., geographic location, the mean absolute normalized differences between the Mie-cloudy and RWP wind speeds are 3.07±2.77, 2.88±2.52 and 3.23±3.39 m/s for categories 1, 2 and 3, respectively. This indicates that the difference in site types has a minor effect on the performance of Mie-cloudy wind products. For Rayleigh-clear wind products, category 3 has the largest difference of 6.2±6.18 m/s between the Rayleigh-clear and RWP wind speed in contrast to small differences of 5.11±4.17 and 5.17±4.62 m/s for categories 1 and 2, respectively, probably indicating that categories 1 and 2 are more suitable to compare with Rayleigh-clear winds than the category 3. The statistical significance difference is also low. Overall, the mean absolute normalized difference (3.06±2.89 m/s) between the Mie-cloudy and RWP wind speeds is smaller than that (5.45±4.97 m/s) between the Rayleigh-clear and RWP wind speeds, indicating that the performance of Mie-cloudy wind products is better than that of Rayleigh-clear wind products. This may be expected from the lower than anticipated atmospheric Aeolus return (Kanitz et al., 2020).

4 Conclusions

An initial comparison between the latest version Aeolus wind products and wind observations from the radar wind profiler network in China during the period 20 April 2020 to 20 July 2020 is presented. Differences between Aeolus HLOS and RWP winds may be due to Aeolus and RWP errors and due to how RWP represents the Aeolus winds in terms of spatial and temporal aggregation. The latter will cause differences in case of heterogenic atmospheric optical and dynamic conditions (Sun et al., 2014). We note that atmospheric heterogeneity may differ for ascending (18:00 LST) and descending (06:00 LST) Aeolus orbits due to the daily atmospheric cycle over land.

According to the location of each RWP site over China relative to the closest Aeolus ground tracks, all the RWP sites are grouped into three matchup categories. The spatial distribution of the RWP sites belonging to categories 1 and 2 indicates that most of the RWP sites over China satisfy set criteria for collocation with Aeolus ground tracks. Further comparative analyses suggest that the mean normalized differences between Mie-cloudy and RWP winds for categories 1, 2, and 3 are −0.33, −0.26, and −0.55 m/s, respectively, thereby demonstrating that different categories do not essentially affect the performance of Mie-cloudy wind products. Additionally, for Rayleigh-clear wind products the bias differences between the different categories are statistically insignificant. The vertical distributions of differences between Mie-cloudy or Rayleigh-clear channels and RWP wind profiles show that the wind differences are generally well below 2 m/s, except for the Rayleigh-clear winds in the height range of 0−1 km. This is due to the Rayleigh performance is limited by received power. From the perspective of observation time, the mean absolute normalized difference between Mie-cloudy (Rayleigh-clear) and RWP winds are 3.06 (5.45), 2.79 (4.81), and 3.32 (5.72) m/s at all times of the day and ascending, and descending orbits, respectively. It therefore appears that the observation time has a minor effect on the HLOS comparison, and the wind product~~s~~ for ascending orbits is slightly superior to that for descending orbits. As for the differences at varying geographical locations, the Aeolus Mie-cloudy and Rayleigh-clear wind products are consistent with RWP wind observations in most regions of east China. The value of R between Mie-cloudy (Rayleigh-clear) and RWP winds is 0.94 (0.81), suggesting that most of the Aeolus wind measurements agree with RWP wind observations according to expectations. Seasonal and regional analyses were not discussed in this study and further work in this respect is needed as more Aeolus winds become available.

Data availability

The radar wind profiler data used in this paper can be provided for non-commercial research purposes upon request (Dr. Jianping Guo: jpguocams@gmail.com). The Aeolus dataset can be downloaded from https://aeolus-ds.eo.esa.int/oads/access/collection (last accessed 24 July 2020). Instructions for use and data download methods can be found on the official website.

Author contributions

The study was completed with close cooperation between all authors. J. Guo and B. Liu conceiv~~design~~ed of the idea for assessing the radar wind profiler data in China; J. Guo and B. Liu conducted the data analyses and co-wrote the manuscript; Y. Zhang, L. Shi, Y. Ma, W. Gong, J. Zhang, A. Stoffelen, G. Leeuw and X. Xu discussed the experimental results, and all coauthors helped reviewing the manuscript and the revisions.

Competing interests.

The authors declare that they have no conflict of interest.

Acknowledgements.

We are very grateful to the China Meteorological Administration for operation and maintenance of the radar wind profiler observational network. This work was financially supported by the National Key Research and Development Program of China under grants 2017YFC0212600 and 2017YFC1501401, and the National Natural Science Foundation of China under grants 41771399, 41401498 and 41627804. The study contributes to the ESA / MOST cooperation project DRAGON5, Topic 3 Atmosphere, sub-topic 3.2 Air-Quality and the ESA Aeolus DISC project.

References

Albertema, S.: Validation of Aeolus satellite wind observations with aircraft-derived wind data and the ECMWF NWP model for an enhanced understanding of atmospheric dynamics, Master thesis Utrecht Un., the Netherlands, 2019 (https://dspace.library.uu.nl/handle/1874/383392).

Ansmann, A., Wandinger, U., Le Rille, O., Lajas, D., and Straume, A.: Particle backscatter and extinction profiling with the spaceborne high-spectral-resolution Doppler lidar ALADIN: methodology and simulations. Appl. Optics, 46, 6606–6622, 2007.

Benjamin, S. G., Schwartz, B. E., Szoke, E. J., and Koch, S. E.: The value of wind profiler data in US weather forecasting. Bulletin of the American Meteorological Society, 85(12), 1871-1886, 2004.

Bentamy, A., Queffeulou, P., Quilfen, Y., and Katsaros, K.: Ocean surface wind fields estimated from satellite active and passive microwave instruments. IEEE transactions on geoscience and remote sensing, 37(5), 2469–2486, 1999.

Belmonte Rivas, M. and Stoffelen, A.: Characterizing ERA-Interim and ERA5 surface wind biases using ASCAT, Ocean Sci., 15, 831–852, https://doi.org/10.5194/os-15-831-2019, 2019.

Constantinescu, E.M., Zavala, V.M., Rocklin, M., Lee, S., and Anitescu, M.: Unit commitment with wind power generation: integrating wind forecast uncertainty and stochastic programming (No. ANL/MCS-TM-309). Argonne National Lab. (ANL), Argonne, IL, United States, 2009.

Dabas, A., Denneulin, M.L., Flamant, P., Loth, C., Garnier, A. and Dolfi-Bouteyre, A.: Correcting winds measured with a Rayleigh Doppler lidar from pressure and temperature effects, Tellus A 60, 206-215. doi:10.1111/j.1600-0870.2007.00284.x. 2008.

Draper, D. W., and Long, D. G. An assessment of SeaWinds on QuikSCAT wind retrieval. Journal of Geophysical Research: Oceans, 107(C12), 107(C12), 3212, doi:10.1029/2002JC001330, 2002.

Ding, A., Nie, W., Huang, X., Chi, X., Sun, J., Kerminen, V. M., ... & Kulmala, M.: Long-term observation of air pollution-weather/climate interactions at the SORPES station: a review and outlook. Frontiers of Environmental Science & Engineering, 10(5), 15, 2016.

De Kloe, J., Stoffelen, A., Tan, D., Andersson, E., Rennie, M., Dabas, A., Poli, P., and Huber, D.: ADM-Aeolus Level-2B/2C Processor Input/Output Data Definitions Interface Control Document, Tech. rep., AE-IF-ECMWF-L2BP-001, v. 3.0, 100 pp., 2017.

European Space Agency (ESA): "ADM-Aeolus Science Report," ESA SP-1311, 121 p., http://esamultimedia.esa.int/docs/SP-1311_ADM-Aeolus_FINAL_low-res.pdf, 2008.

European Space Agency (ESA): “ADM-Aeolus Mission Requirements Document”, ESA EOP-SM/2047, 57 p., http://esamultimedia.esa.int/docs/EarthObservation/ADM-Aeolus_MRD.pdf, 2016.

Flamant, P., Cuesta, J., Denneulin, M. L., Dabas, A., and Huber, D.: ADM-Aeolus retrieval algorithms for aerosol and cloud products. Tellus A: Dyn. Meteorol. Oceanogr., 60, 273–286, https://doi.org/10.1111/j.1600-0870.2007.00287.x, 2008.

Guo, J., Miao, Y., Zhang, Y., Liu, H., Li, Z., Zhang, W., He, J., Lou, M., Yan, Y., Bian, L., and Zhai, P.: The climatology of planetary boundary layer height in China derived from radiosonde and reanalysis data. Atmos. Chem. Phys. 16, 13309, doi:10.5194/acp-16-13309-2016, 2016.

Guo, J., Liu, H., Li, Z., Rosenfeld, D., Jiang, M., Xu, W., Jiang, J. H., He, J., Chen, D., Min, M., and Zhai, P., 2018. Aerosol-induced changes in the vertical structure of precipitation: a perspective of TRMM precipitation radar. Atmos. Chem. Phys., 18, 13329–13343, doi:10.5194/acp-18-13329-2018, 2018.

Guo, J., T. Su, D. Chen, J. Wang, Z. Li, Y. Lv, X. Guo, H. Liu, M. Cribb, and P. Zhai: Declining summertime local-scale precipitation frequency over China and the United States, 1981–2012: The disparate roles of aerosols. Geophysical Research Letters, 46(22), 13281–13289. doi: 10.1029/2019GL085442, 2019.

Houchi, K., Stoffelen, A., Marseille, G. J., and De Kloe, J.: Comparison of wind and wind shear climatologies derived from high-resolution radiosondes and the ECMWF model, *J. Geophys. Res.*, 115, D22123, doi:10.1029/2009JD013196, 2010.

Huuskonen, A., Saltikoff, E., and Holleman, I.: The operational weather radar network in Europe. Bulletin of the American Meteorological Society, 95(6), 897–907, 2014.

Huang, J., Ma, J., Guan, X., Li, Y., & He, Y.: Progress in semi-arid climate change studies in China. Adv.~~ances in~~ Atmos~~pheric.~~. Sci~~ences.~~., 36(9), 922-937, 2019.

Huang, X., Ding, A., Gao, J., Zheng, B., Zhou, D., Qi, X et al.: ~~., ... & Chi, X. (2020).~~ Enhanced secondary pollution offset reduction of primary emissions during COVID-19 lockdown in China. Nat. ~~ional~~ Sci. ~~ence~~ Rev.~~iew,~~ , ~~.~~13(6): 1-7, 2020.

Huang, X., Ding, A., Wang, Z., Ding, K., Gao, J., Chai, F., and~~&~~ Fu, C.: Amplified transboundary transport of haze by aerosol–boundary layer interaction in China. Nature Geoscience, 1-7, 2020.

He, G., Pan, Y., and~~&~~ Tanaka, T. ~~(2020).~~ The short-term impacts of COVID-19 lockdown on urban air pollution in China. Nature Sustainability, 1-7, 2020.~~.~~

Kanitz, T., Witschas, B., Marksteiner, U., Flament, T., Rennie, M., Schillinger, M., Parrinello, T., Wernham, D., and Reitebuch, O.: ESA's Wind Lidar Mission Aeolus – Instrument Performance and Stability, EGU General Assembly 2020, Online, 4–8 May 2020, EGU2020-7146, 2020, https://doi.org/10.5194/egusphere-egu2020-7146.

King, G. P., Portabella, M., Lin, W., Stoffelen, A.: Correlating extremes in wind and stress divergence with extremes in rain over the Tropical Atlantic, EUMETSAT Ocean and Sea Ice SAF Scientific Report OSI_AVS_15_02, Version 1.0, 13 November 2017, http://www.osi-saf.org/?q=content/correlating-extremes-wind-and-stress-divergence-extremes-rain-over-tropical-atlantic.

Marksteiner, U., Lemmerz, C., Lux, O., Rahm, S., Schäfler, A., Witschas, B., and Reitebuch, O.: Calibrations and Wind Observations of an Airborne Direct-Detection Wind LiDAR Supporting ESA's Aeolus Mission, Remote Sensing, 10, 2056, https://doi.org/10.3390/rs10122056, 2018

Michelson, S.A., and Bao, J.W.: Sensitivity of low-level winds simulated by the WRF model in California's Central Valley to uncertainties in the large-scale forcing and soil initialization. Journal of Applied Meteorology and Climatology, 47(12), 3131–3149, 2008.

Nash, J., and Oakley, T. J.: Development of COST 76 wind profiler network in Europe. Physics and Chemistry of the Earth, Part B, 3(26), 193–199, 2001.

Lebo, Z. J., and Morrison, H.: Dynamical effects of aerosol perturbations on simulated idealized squall lines. Monthly Weather Review, 142(3), 991-1009, 2014.

Li, Z., Niu, F., Fan, J., Liu, Y., Rosenfeld, D., and Ding, Y.: Long-term impacts of aerosols on the vertical development of clouds and precipitation. Nature Geoscience, 4(12), 888-894, 2011.

Le, T., Wang, Y., Liu, L., Yang, J., Yung, Y. L., Li, G., and~~&~~ Seinfeld, J. H.: ~~(2020).~~ Unexpected air pollution with marked emission reductions during the COVID-19 outbreak in China. Science, 369(6504), 702-706, 2020.~~.~~

Liu, B., Ma, Y., Gong, W., Zhang, M., and Yang, J.: Study of continuous air pollution in winter over Wuhan based on ground-based and satellite observations. Atmospheric Pollution Research, 9(1), 156-165, 2018.

Liu, B., Ma, Y., Guo, J., Gong, W., Zhang, Y., Mao, F., Li, J., Guo, X., and Shi, Y.: Boundary layer heights as derived from ground-based Radar wind profiler in Beijing. IEEE ~~Transactions~~ Trans.~~on~~ Geosci.~~ence and~~ Remote Sens.~~ing~~, 57 (10), 8095–8104. doi: 10.1109/TGRS.2019.2918301, 2019.

Liu, B., Guo, J., Gong, W., Shi, Y., and Jin, S.: Boundary l~~L~~ayer h~~H~~eight as e~~E~~stimated from Radar w~~W~~ind p~~P~~rofilers in f~~F~~our c~~C~~ities in China: Relative c~~C~~ontributions from Aerosols and s~~S~~urface f~~F~~eatures. Remote Sens.~~ing~~, 12(10), 1657, 2020a.

Liu, B., Guo, J., Gong, W., Shi, L., Zhang, Y., and Ma, Y.: Characteristics and performance of vertical winds as observed by the radar wind profiler network of China. Atmos. Meas. Tech., doi:10.5194/amt-2020-75, 2020b.

Liu, H., J. He, J. Guo, Y. Miao, J. Yin, Y. Wang, H. Xu, H. Liu, Y. Yan, Y. Li, P. Zhai: The blue skies in Beijing during APEC 2014: A quantitative assessment of emission control efficiency and meteorological influence. Atmos. Environ. 167: 235–244, 2017.

Lux, O., Lemmerz, C., Weiler, F., Marksteiner, U., Witschas, B., Rahm, S., Schäfler, A., and Reitebuch, O.: Airborne wind lidar observations over the North Atlantic in 2016 for the pre-launch validation of the satellite mission Aeolus. Atmos. Meas. Tech., 11, 3297–3322, doi:10.5194/amt-11-3297-2018, 2018

Lux, O., Lemmerz, C., Weiler, F., Marksteiner, U., Witschas, B., Rahm, S., Geiß, A., and Reitebuch, O.: Intercomparison of wind observations from the European Space Agency's Aeolus satellite mission and the ALADIN Airborne Demonstrator. Atmos. Meas. Tech., 13(4), 2020.

Marseille, G.-J. and Stoffelen, A.: Simulation of wind profiles from a space-borne Doppler wind lidar. Q. J. R. Meteorol. Soc., 129, 3079–309, 2003.

Pu, Z., Zhang, L., and Emmitt, G. D.: Impact of airborne Doppler wind lidar profiles on numerical simulations of a tropical cyclone, Geophys. Res. Lett., 37, L05801, doi:10.1029/2009GL041765, 2010.

Reitebuch, O., Huber, D., and Nikolaus, I.: Algorithm Theoretical Basis Document ATBD: ADM-Aeolus Level 1B Products, v. 4.4, 117 pp., 2018

Reitebuch, O.: The Spaceborne Wind Lidar Mission ADM-Aeolus, in: Atmospheric Physics, edited by: Schumann, U., Springer Berlin, Heidelberg, 487–507, 2012.

Rennie, M. P. and Isaksen, L.: An Assessment of the Impact of Aeolus Doppler Wind Lidar Observations for Use in Numerical Weather Prediction at ECMWF, EGU General Assembly 2020, Online, 4–8 May 2020, EGU2020-5340, https://doi.org/10.5194/egusphere-egu2020-5340, 2020.

Rennie, M. P.: An assessment of the expected quality of Aeolus Level-2B wind products, EPJ Web Conf., 176, 02015, https://doi.org/10.1051/epjconf/201817602015, 2018.

Shi, Y., Liu, B., Chen, S., Gong, W., Ma, Y., Zhang, M. et al.: Characteristics of aerosol within the nocturnal residual layer and its effects on surface $PM_{2.5}$ over China. Atmos. Environ., 241, 117841, 2020.

Simonin, D., Ballard, S. P., and Li, Z. Doppler radar radial wind assimilation using an hourly cycling 3D-Var with a 1.5 km resolution version of the Met Office Unified Model for nowcasting. Quarterly Journal of the Royal Meteorological Society, 140(684), 2298-2314, 2014.

Stettner, D., Velden, C., Rabin, R., Wanzong, S., Daniels, J., and Bresky, W.: Development of enhanced vortex-scale atmospheric motion vectors for hurricane applications. Remote Sens.~~ing~~, 11(17), 1981, 2019.

Stoffelen, A., A. Benedetti, R. Borde, A. Dabas, P. Flamant, M. Forsythe, M. Hardesty, L. Isaksen, E. Källén, H. Körnich, T. Lee, O. Reitebuch, M. Rennie, L. Riishøjgaard, H. Schyberg, A. G. Straume, and M. Vaughan: Wind profile satellite observation requirements and capabilities. Bull. Amer. Meteor. Soc., https://doi.org/10.1175/BAMS-D-18-0202.1, 2020.

Stoffelen A., Kumar R., Zou J., Karaev V., Chang P.S., Rodriguez E. Ocean Surface Vector Wind Observations. In: Barale V., Gade M. (eds) Remote Sensing of the Asian Seas. Springer, Cham. https://doi.org/10.1007/978-3-319-94067-0_24, 2019.

Stoffelen, A., Pailleux, J., Källén, E., Vaughan, J. M., Isaksen, L., Flamant, P., Wergen, W., Andersson, E., Schyberg, H., Culoma, A., Meynart, R., Endemann, M., and Ingmann, P.: The atmospheric dynamics mission for global wind field measurement. B. Am. Meteorol. Soc., 86, 73–88, 2005.

Sun, X. J., Zhang, R. W., Marseille, G. J., Stoffelen, A., Donovan, D., Liu, L., and Zhao, J.: The performance of Aeolus in heterogeneous atmospheric conditions using high-resolution radiosonde data, Atmos. Meas. Tech., 7, 2695–2717, https://doi.org/10.5194/amt-7-2695-2014, 2014.

Su, T., Li, Z., Zheng, Y., Luan, Q., and Guo, J.: Abnormally shallow boundary layer associated with severe air pollution during the COVID-19 lockdown in China. Geophys. Res. Lett., 47, e2020GL090041. https://doi.org/10.1029/2020GL090041, 2020.

Tan, D. G. H., Andersson, E., de Kloe, J., Marseille, G., Stoffelen, A., Poli, P., Denneulin, M., Dabas, A., Huber, D., Reitebuch, O., Flamant, P., Le Rille, O., and Nett, H.: The ADM-Aeolus wind retrieval algorithms. Tellus A, 60, 191–205, 2008.

Tan, D., Rennie, M., Andersson, E., Poli, P., Dabas, A., de Kloe, J., Marseille, G.-J., and Stoffelen, A.: Aeolus Level-2B Algorithm Theoretical Basis Document, Tech. rep., AE-TN-ECMWFL2BP-0023, v. 3.0, 109 pp., 2017.

Weissmann, M. and Cardinali, C.: Impact of airborne Doppler lidar observations on ECMWF forecasts. Q. J. Roy. Meteor. Soc., 133, 107–116, 2007.

Witschas, B., Lemmerz, C., Geiß, A., Lux, O., Marksteiner, U., Rahm, S., Reitebuch, O., and Weiler, F.: First validation of Aeolus wind observations by airborne Doppler wind lidar measurements. Atmospheric Measurement Techniques, 13(5), 2381–2396, 2020.

Witschas,B., Vieitez, M. O., van Duijn, E.-J., Reitebuch, O., van de Water, W., and Ubachs, W.: Spontaneous Rayleigh–Brillouin scattering of ultraviolet light in nitrogen, dry air, and moist air, Applied Optics, 49(22), 2010.

Winker, D. M., Vaughan, M. A., Omar, A., Hu, Y., Powell, K. A., Liu, Z., Hunt, W. H., and Young, S. A.: Overview of the CALIPSO mission and CALIOP data processing algorithms, J. Atmos. Ocean. Tech., 26, 2310–2323, 2009

Yang, Y., Yim, S.H., Haywood, J., Osborne, M., Chan, J.C., Zeng, Z. and Cheng, J.C.: Characteristics of heavy particulate matter pollution events over Hong Kong and their relationships with vertical wind profiles using high-time-resolution Doppler lidar measurements. Journal of Geophysical Research: Atmospheres, 124(16), 9609-9623, 2019.

Zhang, R., Li, Q., and Zhang, R.: Meteorological conditions for the persistent severe fog and haze event over eastern China in January 2013. Science China Earth Sciences, 57(1), 26-35, 2014.

Zhang, Y., J. Guo, Y. Yang, Y. Wang, and S.H.L. Yim: Vertical wind shear modulates particulate matter pollutions: A perspective from Radar wind profiler observations in Beijing, China. Remote Sensing, 12(3), 546. https://doi.org/10.3390/rs12030546, 2020.

Zhai, X., Marksteiner, U., Weiler, F., Lemmerz, C., Lux, O., Witschas, B., and Reitebuch, O.: Rayleigh wind retrieval for the ALADIN airborne demonstrator of the Aeolus mission using simulated response calibration. Atmos. Meas. Tech., 13, 445–465, https://doi.org/10.5194/amt-13-445-2020, 2020.

Tables:

Table 1. Summary of the collocation categories used in this study: position of RWP sites relative to the nearest Aeolus ground tracks, calculated based on a 75-km-radius circle centred at each RWP site.

Category	No. of Aeolus ground tracks	Shortest distance (km)	No. of sites
1	2	0–37.5	32
2	1	0–37.5	39
3	1	37.5–75	38

Figures:

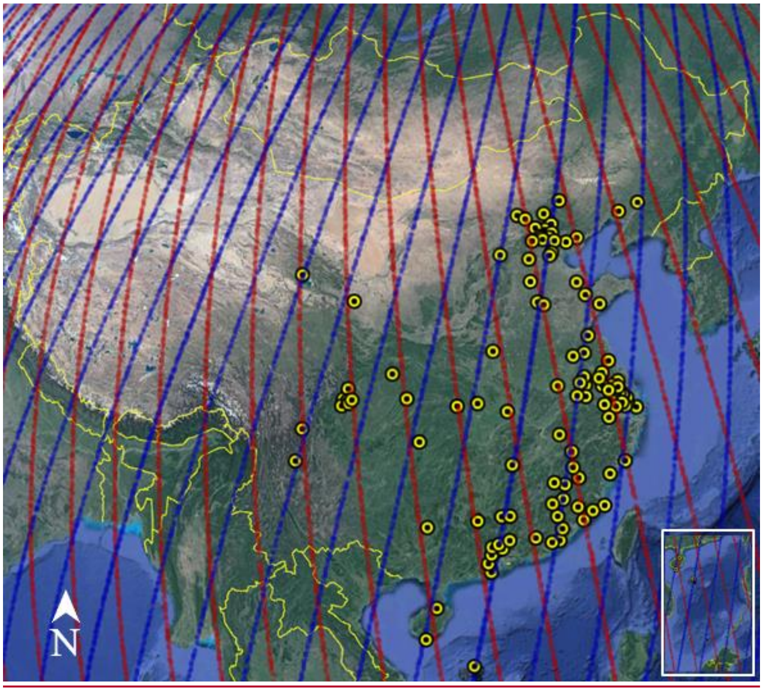

Figure 1. Geographic distribution of RWP sites and Aeolus ground tracks superimposed on the GoogleEarth map of China (© Google Maps). Red and blue lines represent the Aeolus ground tracks for ascending and descending orbits, respectively. The yellow dots denote the RWP sites.

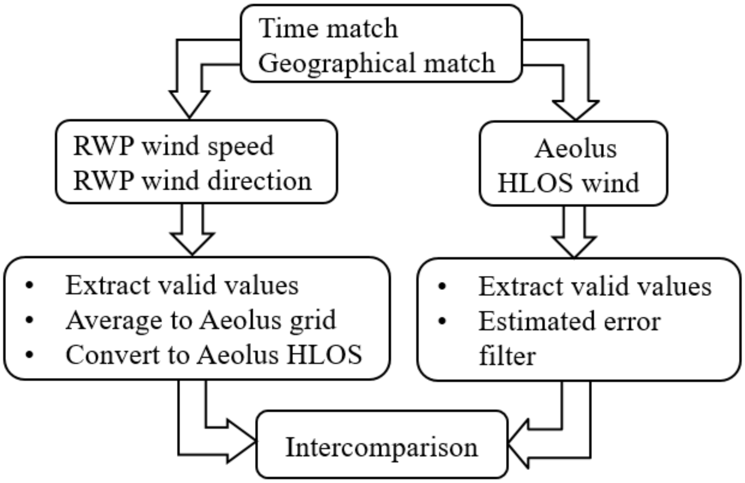

Figure 2. Flowchart of the processing procedures used to compare the RWP observations with Aeolus observations.

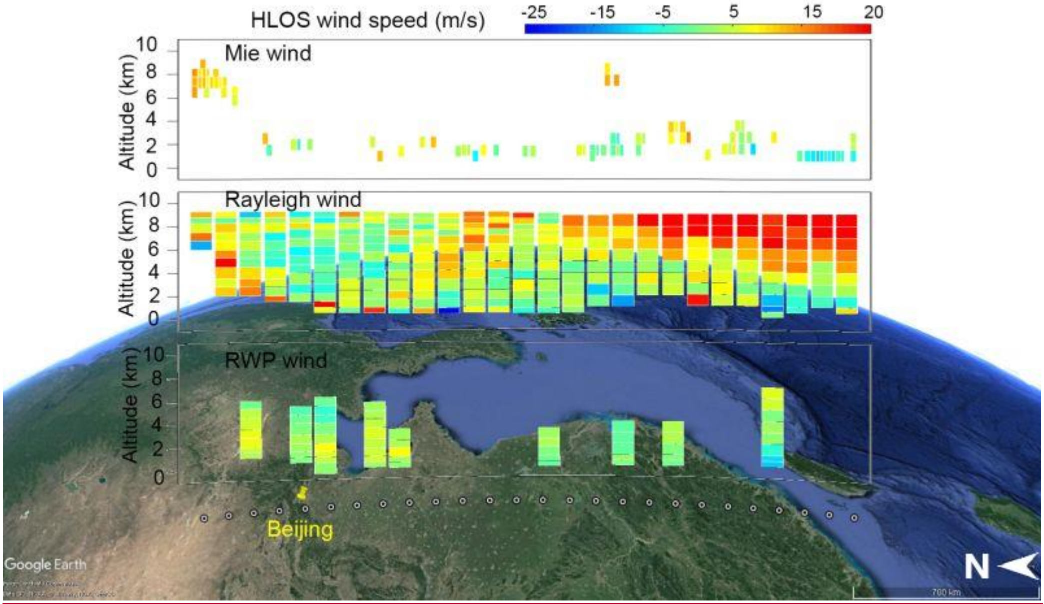

Figure 3. Case study of HLOS wind component profiles on 28 April 2020 between 21.5 °N and 43.5 °N superimposed on the GoogleEarth map of east China (© Google Maps). The top, middle and bottom panels show Mie-cloudy, Rayleigh-clear, and RWP wind profiles, respectively. Color bar represents the HLOS wind vector component in m s^{-1}.

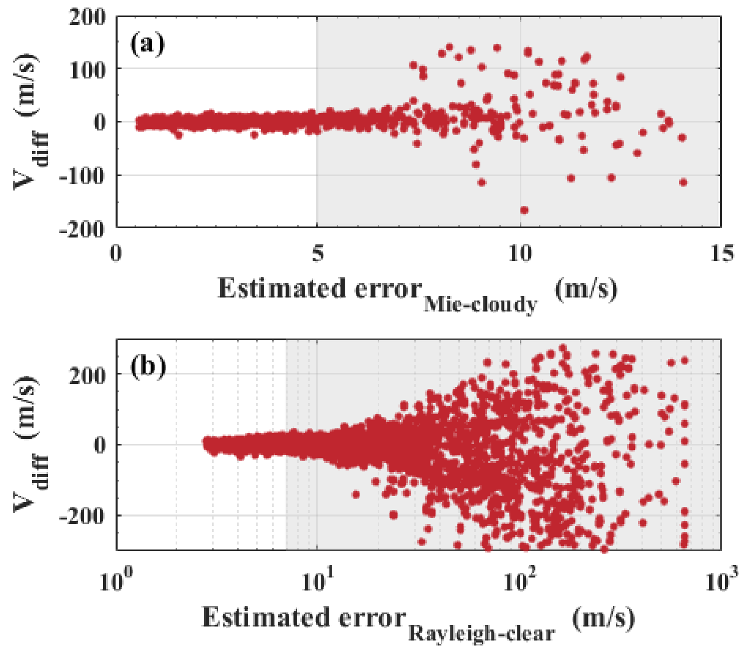

Figure 4. Difference between the Aeolus HLOS and RWP HLOS wind components as a function of estimated errors for (a) Mie-cloudy winds and (b) Rayleigh-clear winds. Gray areas indicate the data with errors larger than 7 m/s (Rayleigh) or 5 m/s (Mie), which in the present analysis are considered as invalid observations.

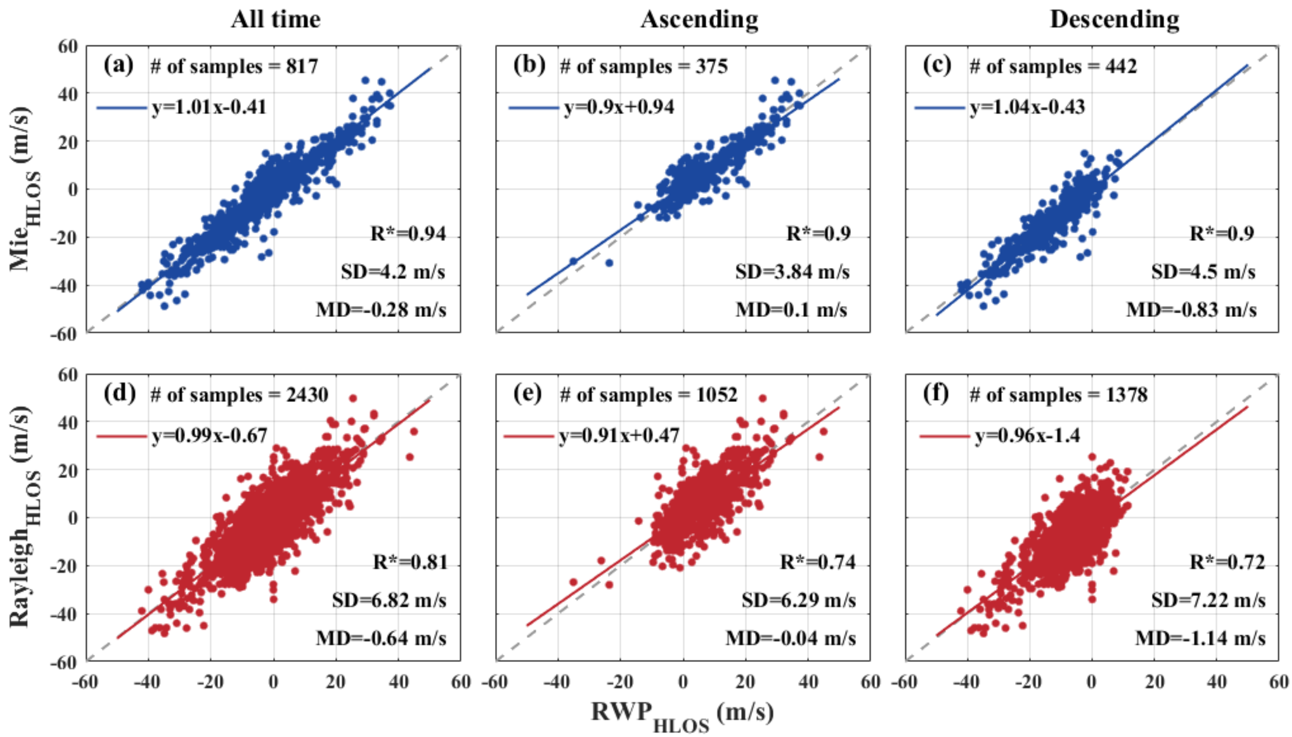

Figure 5. Aeolus against RWP HLOS winds for (a, b, c) Mie-cloudy winds and (d, e, f) Rayleigh-clear winds for (a,d) all data and (b,e) ascending and (c,f) descending orbits. Corresponding least-square line fits are indicated by the solid lines. The fit results are shown in the insets. The 1:1 line is represented by the gray dashed line.

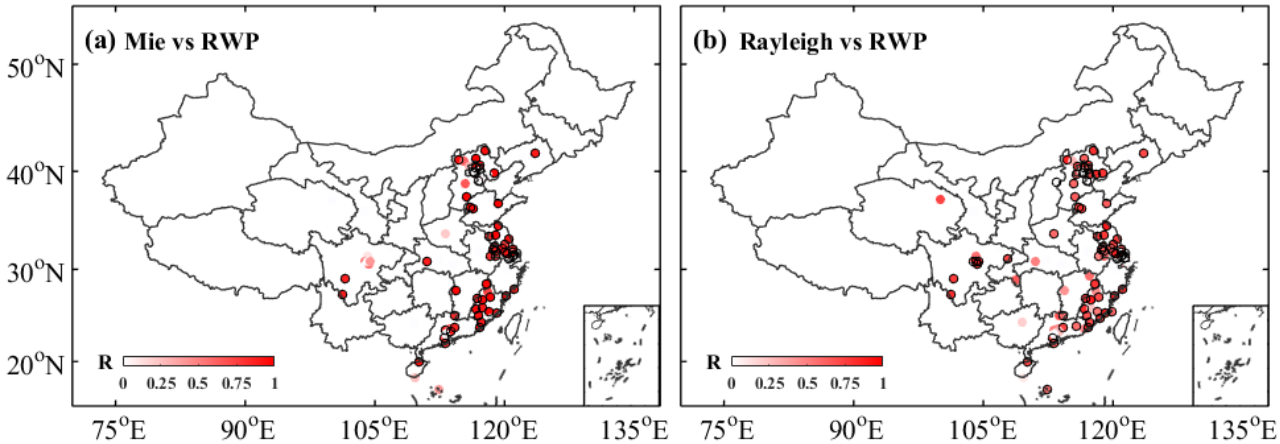

Figure 6. Correlation coefficients between Aeolus HLOS and RWP HLOS wind speeds. The wind measurements are separated in (a) Mie-cloudy winds and (b) Rayleigh-clear winds. The black circles indicate that the site passed the significance test ($P<0.05$).

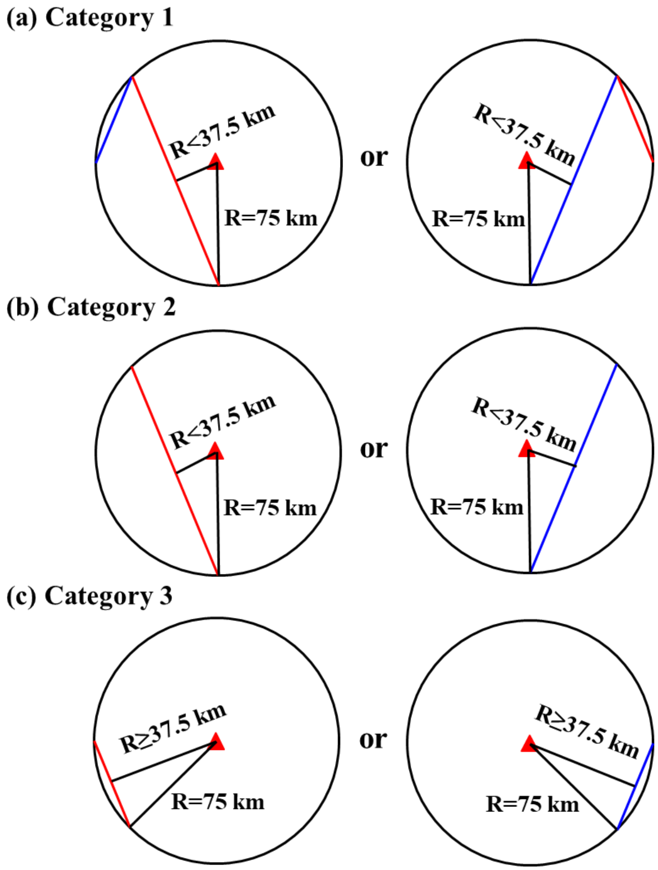

Figure 7. Schematic diagrams of three categories showing the location of Aeolus ground tracks relative to the RWP sites which are based on a circle with a radius of 75 km centered at the RWP sites (red triangle) to match the Aeolus and RWP wind observations: (a) Category 1, (b) Category 2, and (c) Category 3, in which the shortest distance from ascending (red line) or descending (blue line) Aeolus ground track to its nearest RWP site is less or greater than 37.5 km.

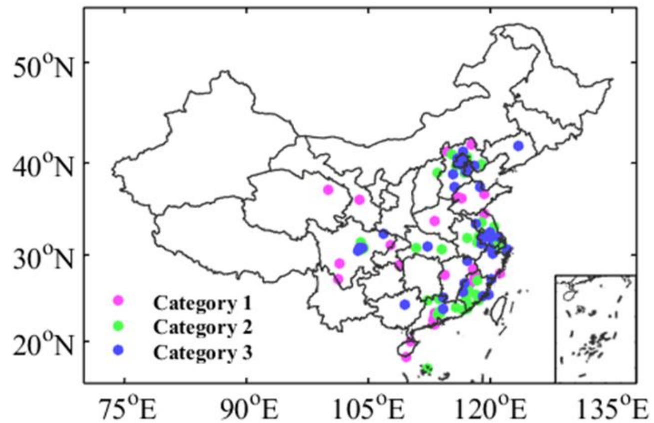

Figure 8. Geographical distribution of RWP sites relative to Aeolus ground tracks over China. The cyan, green, and blue solid circles correspond to categories 1, 2, and 3 as displayed in Fig. 5.

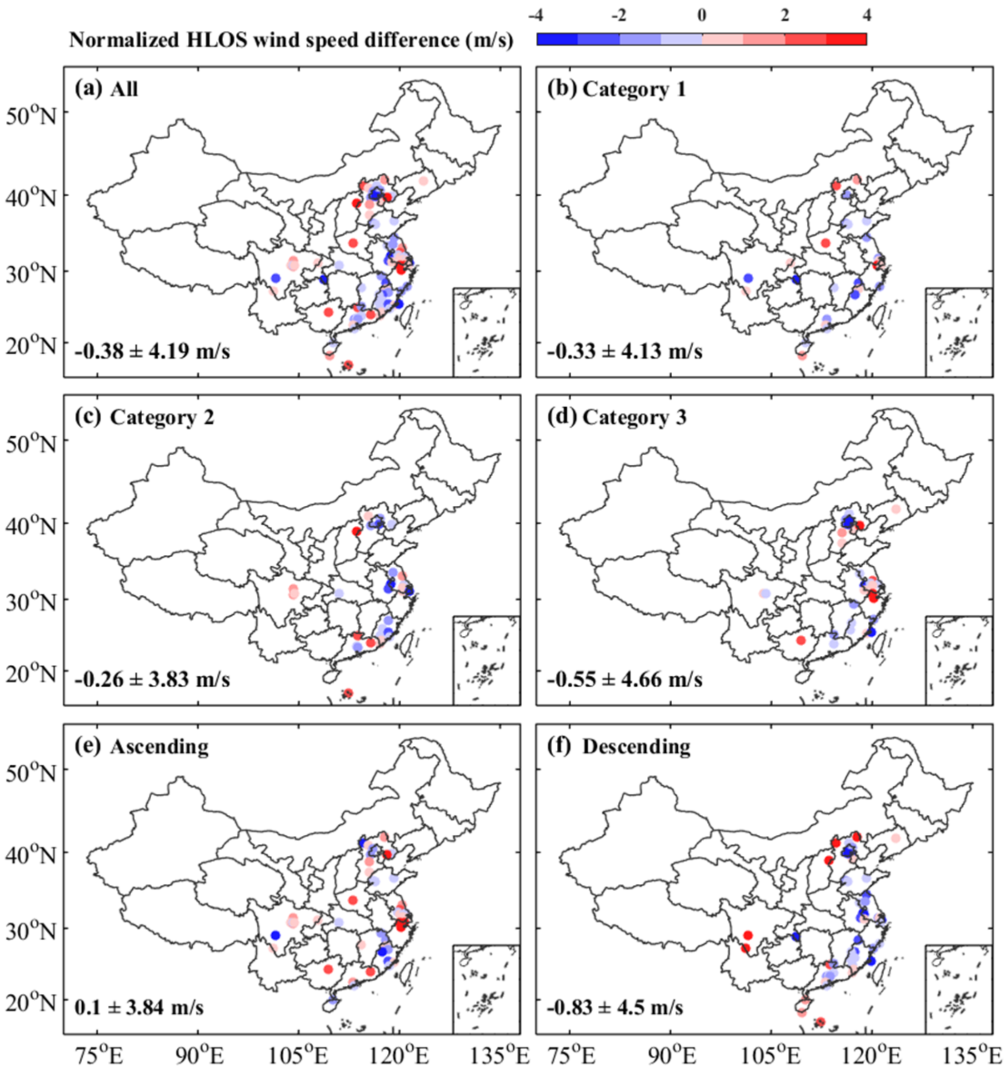

Figure 9. The geographic distribution of the normalized differences between the Aeolus HLOS and the RWP HLOS wind speeds for Mie-cloudy winds. The normalized differences are shown for all RWP sites in China (a) and for the RWP sites belonging to (b) Category 1, (c) Category 2, (d) Category 3, (e) ascending, and (f) descending. The text labels represent the mean difference and standard deviation. The black circles indicate that the site passed the statistical significance difference test ($P<0.05$).

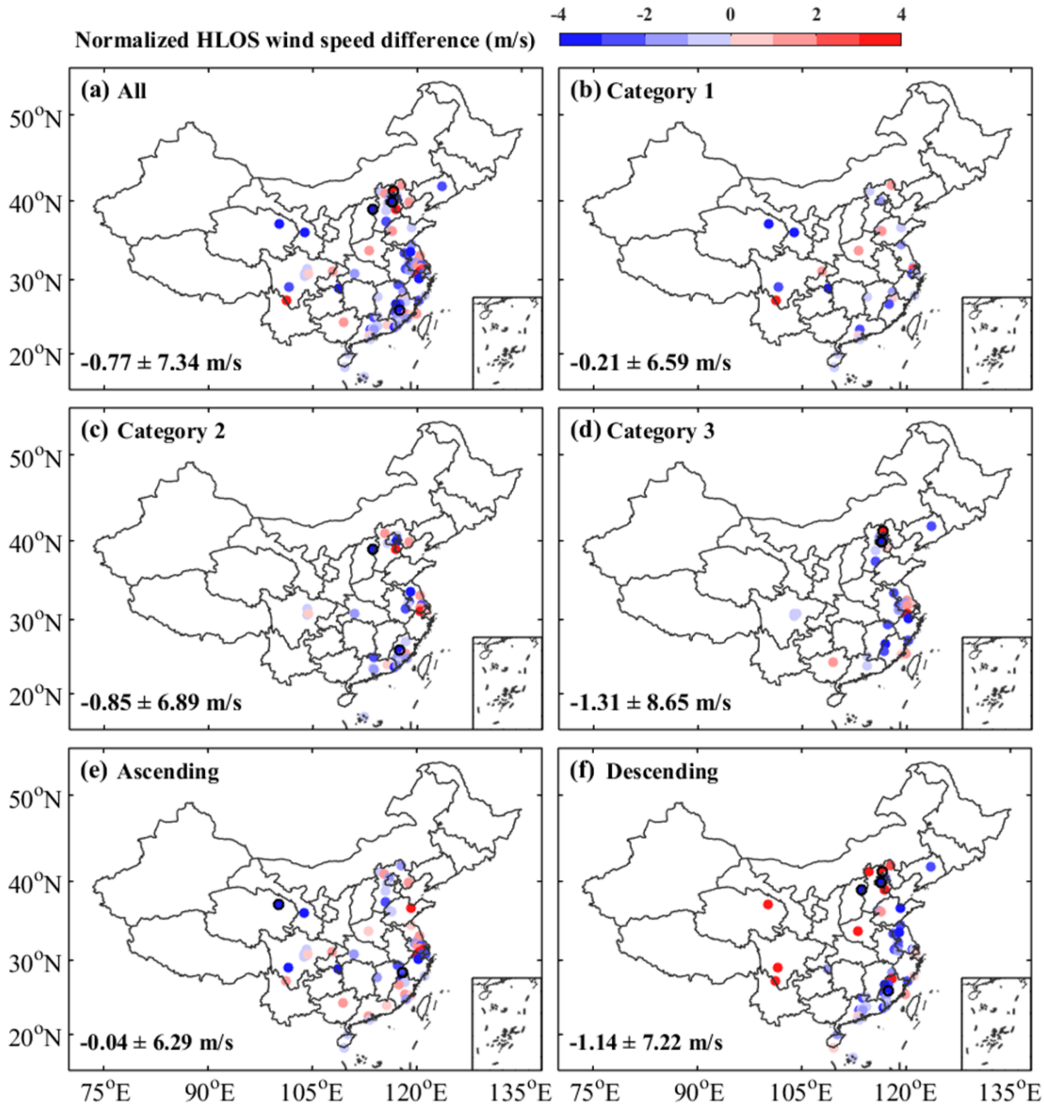

Figure 10. Same as Fig. 9, but for Rayleigh-clear winds.

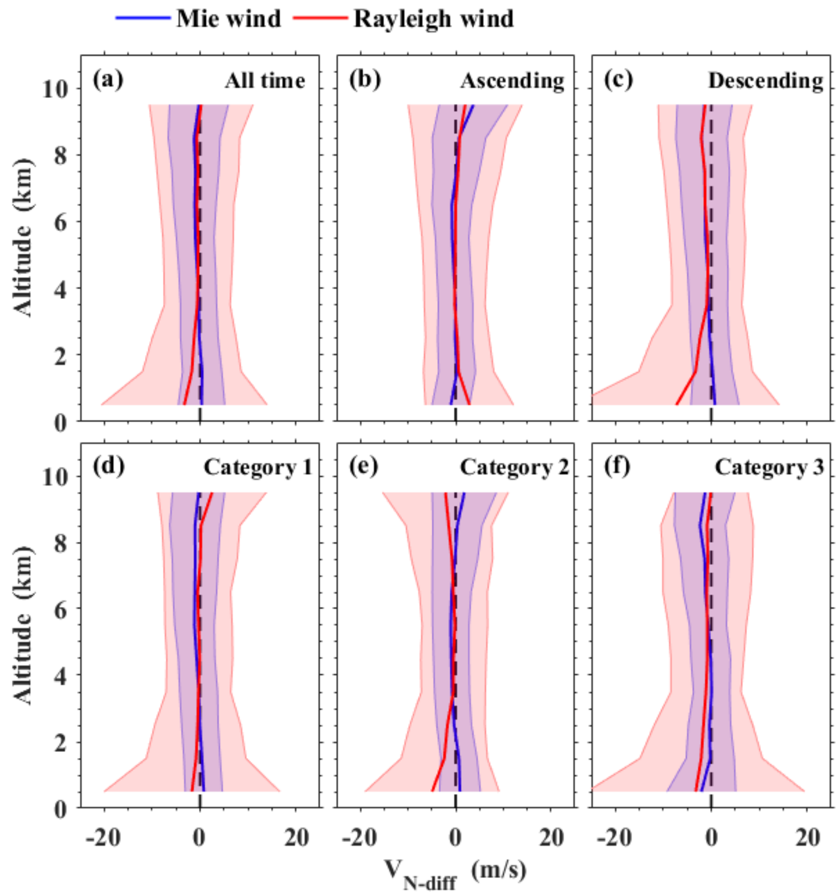

Figure 11. Vertical distributions of the normalized differences between the Aeolus HLOS and RWP HLOS wind speeds for (a) all time, (b) ascending, (c) descending, (d) Category 1, (e) Category 2, and (f) Category 3. Blue and red lines represent Mie-cloudy and Rayleigh-clear wind, respectively. Corresponding color shading areas represent one standard deviation to each side of the mean normalized difference.

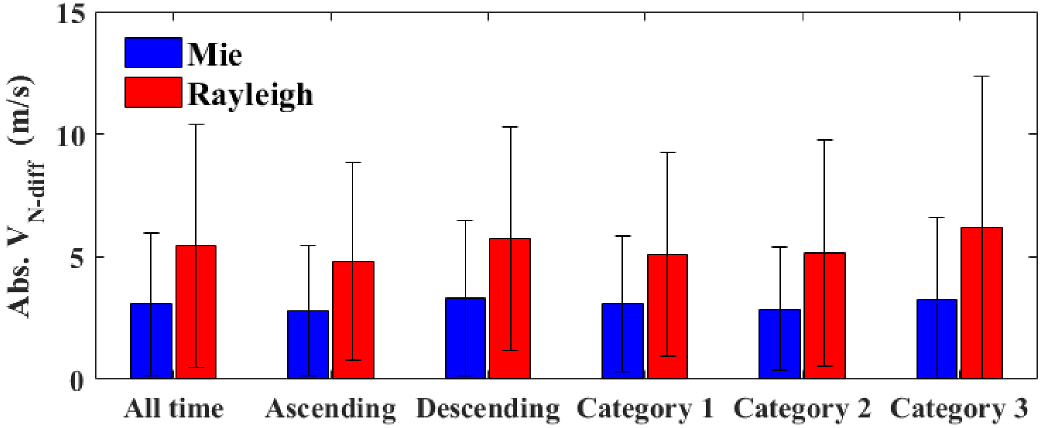

Figure 12. Absolute normalized differences between Aeolus HLOS and RWP HLOS wind speeds for Mie-cloudy winds (blue bar) and Rayleigh-clear winds (orange bar). The thin black range indicates a spread of absolute normalized difference standard deviations.